Thermal Decomposition Studies of Energetic Materials Using Confined Rapid Thermolysis / FTIR Spectroscopy

E. S. KIM, H. S. LEE, C. F. MALLERY, and S. T. THYNELL*

Department of Mechanical Engineering, The Pennsylvania State University, University Park, PA 16802

An experimental setup for performing rapid thermolysis studies of small samples of energetic materials is described. In this setup, about 8 μL of a liquid sample or about 2 mg of a solid sample is heated at rates exceeding 1500 K/s to a set temperature where decomposition occurs. The rapid heating is achieved as a result of confining the sample between two closely spaced isothermal surfaces. The gaseous decomposition products depart from the confined space through a rectangular slit into the region of detection. The evolved gases are quantified using FTIR absorption spectroscopy by accounting for the instrument line shape. To illustrate the use of this setup, the thermolysis behaviors of three different energetic materials are examined. These materials include HMX, RDX, and HAN, all of which are considered as highly energetic propellant ingredients. The results obtained in this study of the temporal evolution of species concentrations from these ingredients are in reasonably close agreement with results available in the literature.

INTRODUCTION

During the past decade, significant advancements have been made related to the prediction of the flame structure of solid propellants. Existing modeling techniques are capable of predicting the one-dimensional, steady-state temperature and species distributions within the flame zone, the burn rate, and the temperature sensitivity of the monopropellant cyclotrimethylene trinitramine (RDX) [1, 2]. Currently, the modeling efforts are focused on other monopropellants as well as various binder ingredients. The progress is attributed in part to the availability of detailed gas-phase chemical reaction mechanisms and experimental data for model validation [3]. To improve the predictive ability of existing comprehensive flame structure codes, much more needs to be learned about the thermal decomposition behavior of the propellant ingredients, including kinetic rates and species formed [4, 5].

To study the decomposition behavior of propellant ingredients, it is well established that high heating rates must be achieved. It is common that the propellant experiences heating rates much greater than 1000 K/s, but these rates are strongly linked to the pressure-dependent burn rate. To perform isothermal decomposition studies, it is necessary to raise the temperature of the sample rapidly to the specified level, and then determine the species formed using either intrusive or nonintrusive techniques. This is of particular importance for RDX, which is known to have two general decomposition pathways with different temperature dependence. Realizing the importance of high heating rates, Brill and co-workers have developed several different experimental techniques for studying the condensed-phase decomposition behavior of solid and liquid propellant ingredients [6–8].

In one of their experimental setups, a thin nichrome plate was heated via Joule heating at rates up to about 200 K/s [6]. About 1 mg of the energetic sample was placed near the center of plate, and a thermocouple was spot-welded onto the bottom side of the plate to deduce endo- or exothermicity of the decomposition processes. The nichrome plate was confined within a chamber which could be pressurized up to 6.89 MPa. Optical access through two ZnSe windows was made to a rapid-scanning Fourier transform infrared (FTIR) spectrometer for determining the concentration of the evolved species through an analysis of the spectral absorbance. Since the mass loss is very important to quantify, the simultaneous mass and temperature change/FTIR (SMATCH/FTIR) setup was developed [7]. Recently, the T-jump/FTIR experiment was developed, and it has been used to study a wide variety of energetic samples [8]. In this

* Corresponding author.

COMBUSTION AND FLAME 110: 239–255 (1997)

Published by Elsevier Science Inc.

0010-2180/97/$17.00
PII S0010-2180(97)00062-X

setup, a 12 μm thin, 5 mm wide, and 38 mm long platinum foil is heated electrically to a set temperature. The 200 μg sample is placed at the midpoint of the foil, and species evolve vertically into the cool atmosphere above the foil. The gas-phase species are detected and quantified using rapid-scanning FTIR spectroscopy. In this setup, heating rates on the order of 600 K/s are achievable in an inert environment which can be pressurized up to 6.89 MPa. Besides determining the species evolution, the endo- and exothermicity of the sample are deduced from a measurement of the voltage drop across the foil. The T-jump/FTIR spectroscopic tool has been very valuable for decomposition studies of energetic materials, in particular those which have a low volatility or have a tendency to become attached to the foil. Recently, a model was developed of the T-jump/FTIR experiment in order to deduce the global decomposition rates of condensed-phase decomposition of RDX [9]; the determined rates were subsequently used in self-sustained [1] and laser-assisted flame structure studies [2]. However, it could be quite difficult to study energetic materials which either readily vaporize, have a low propensity to stick to a heated surface, or are catalytically affected by the hot foil. Hence, there appears to be a need to continue the development of new experimental techniques which can be used to perform thermolysis studies of energetic materials at high heating rates.

To increase the residence time of the volatile liquid or nonsticking material within the isothermal region, it is necessary to confine the evolved gases. Thus, a small isothermal volume, which allows for a confined species evolution, must be devised. It is recognized that the pressure must remain constant. The objective of this work is to describe a system which: 1) allows for confinement of the evolved gases, 2) is applicable to reasonably high temperatures, 3) uses species evolution detection from FTIR absorption spectroscopy, and 4) delivers heating rates of the sample which are similar to those in actual propellant burning situations. Its use, approach for quantifying the species evolved, and representative results from decomposition studies of propellant samples are described in the following sections.

EXPERIMENTAL SETUP

A schematic diagram of a portion of the overall experimental setup is shown in Fig. 1. The

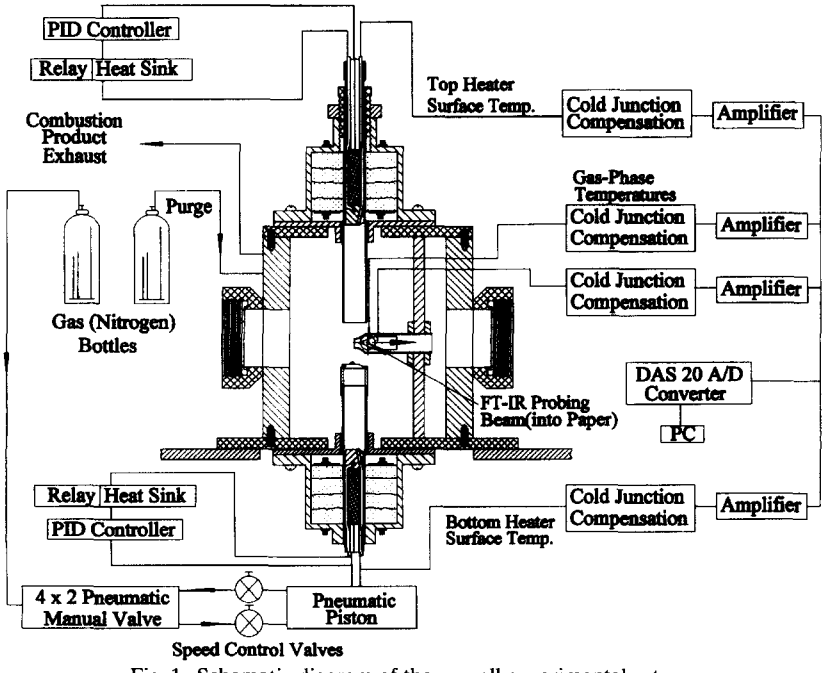

Fig. 1. Schematic diagram of the overall experimental setup.

overall setup consists of the constant-pressure chamber, which is positioned on a rigid frame (not shown), and the Nicolet 740 FTIR spectrometer with its accompanying optics. The overall technique is referred to as confined rapid thermolysis (CRT)/FTIR spectroscopy. One of the main advantages of this technique, achieved by constant contact of the sample with isothermal surfaces, is the rapid heating of an energetic material up to its decomposition temperature at rates exceeding 1500 K/s. The height and inner diameter of the chamber are approximately 23.8 and 12.4 cm, respectively. Attached to the chamber are several systems, including one for achieving proportional-integral-derivative (PID) control of the temperature within each heater, a second for recording the voltage output from *K*-type thermocouples located at the interface temperature between foil and heater probe as well as in the gas phase, a third for pneumatically elevating the lower heater, and a fourth for purging the decomposition products from the chamber. Gas-phase species detection is achieved from FTIR absorption spectroscopy. The modulated beam of the FTIR traverses through two ZnSe windows, which allow a spectral coverage from approximately 500 to 10,000 cm^{-1}. This spectral range is reduced by the beamsplitter (germanium coating on a KBr substrate) and the detectivity of the mercury–cadmium–telluride (MCT) detector. As a result, a spectral range in the mid-IR from about 600 to 5000 cm^{-1} is covered; over this spectral range, the rovibrational bands from most IR-active species are present. In test conducted at atmospheric pressures, the FTIR spectrometer is typically configured to acquire spectra at the rate of 0.23 s per spectrum at a spectral resolution of 2 cm^{-1}. The analytical approach for processing of the spectral data is described in detail in the following section. The position of the FTIR spectrometer relative to the decomposition chamber is equivalent to the overall schematic diagram shown in Ref. 10.

Isothermal conditions within each heater probe are achieved by using high-watt density cartridge heaters (Omega CIR-1014/120). Their temperatures are monitored using standard PID controllers (Omega CN8500). Each heater is embedded within a copper rod of 12.5 mm diameter and 45 mm length. The use of copper ensures a highly isothermal system, but an inert purge gas is required to prevent oxidation. Although the set temperature of the heaters is reached within approximately 60 s, the two heaters are located within fiberglass insulation during the heating process in order to prevent preheating of the sample and to reduce heat losses from the heaters to the surroundings, as shown in Fig. 2. Based on this design, decomposition temperatures up to 973 K can be achieved.

Four different temperatures are recorded. As shown in Fig. 3, two *K*-type thermocouples are embedded in each heater probe. One is placed in close vicinity to the cartridge heater for use of its temperature control. The other is positioned at the interface between the heater probe and foil in order to provide an indication of the sample's temperature variation and reveal the endo- or exothermicity of the decomposition process. The temperature of the evolved gas is recorded using two 75 μm *K*-type thermocouples located 3 and 8 mm away from the exit slit. Recording of the voltage output from these thermocouples is achieved by using a standard DAS20 12 bit A/D converter (Metrabyte). To eliminate initial concentrations of H_2O, CO_2, and particulates, the test chamber is purged with nitrogen. A small amount of purge gas flows through the chamber throughout the experiment to prevent the recirculation of decomposition products into the path of the modulated beam of the FTIR spectrometer.

Each experiment involves the use of a small amount of a sample. Typically, about 8 μL of a liquid or 2 mg of a solid is placed on top of the sample holder, as shown in Fig. 2. The sample holder is initially placed on the top of the lower guiding tube. Once the set temperature is reached, the upper heater probe is lowered manually through its guiding tube and is locked in its set position. Subsequently, the lower heater probe is raised using a pneumatic piston (Schrader Bellows) through its guiding tube. During its upward travel, the lower heater probe lifts the sample holder and is raised until it makes firm but spring-loaded contact with the surface of the upper heater probe. At that

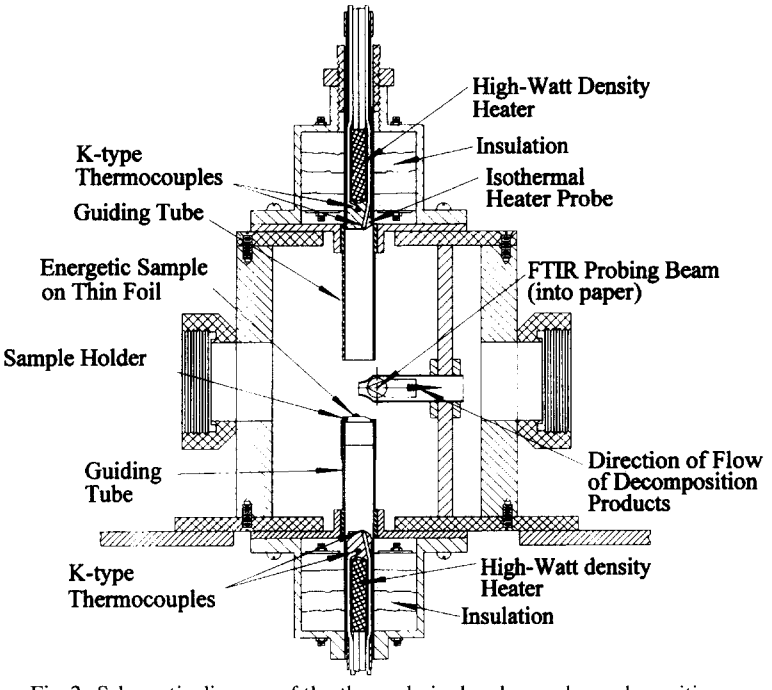

Fig. 2. Schematic diagram of the thermolysis chamber and sample position.

time, there is about a 300 μm gap between the two foils, as shown in Fig. 3. The outer ring, which is attached to the upper heater probe, seals around the periphery of the gap, except for a 6 mm wide and 300 μm high slit through which the evolved gases emerge into the modulated beam of the FTIR. This outer ring is also used to retain the foil on the upper heater probe. The relatively small mass of the sample holder increases the heating rates of the sample. A very small amount of epoxy is used to attach the foil to the sample holder. It is possible to utilize different metal foils. Typically, 11 μm thick aluminum or 6 μm thick SS304 foil is used. Due to the foil's thinness, its resistance to conductive heat transfer is quite small compared to contact or convective resistance between the foil and the sample.

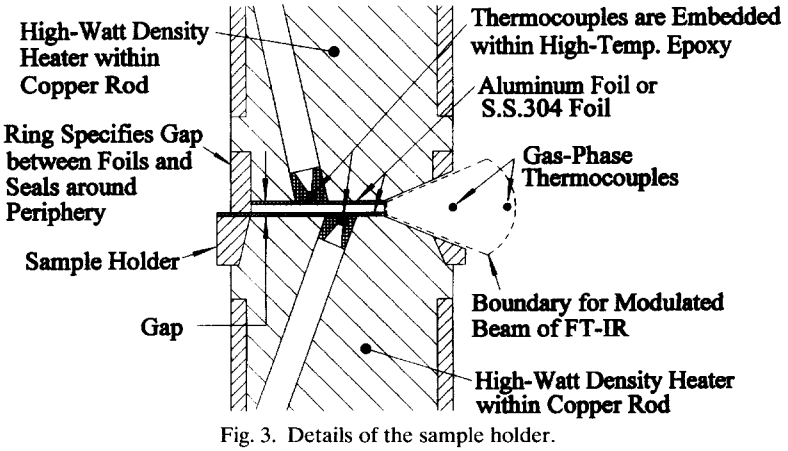

Fig. 3. Details of the sample holder.

There are several concerns with this setup that require further discussion. First, since the volume is large compared to the area of the exit slit through which the evolved gases depart, it may be possible that the pressure builds up during a rapid decomposition event. However, to acquire spectral data, one is required to study an event which lasts several seconds. It is easy to show that, for such a relatively long event, the exit velocities of the evolved gases are on the order of 1 m/s, which suggests that the pressure must remain close to ambient conditions. Second, no build-up of gases occurs within the volume occupied by the modulated beam of the FTIR because of the "large" exit velocity of the evolved gases. Finally, by using metal foils, there are concerns of catalytic effects. The catalytic effects of a wide variety of energetic materials in the condensed phase and various metal substrates were investigated by Brill and co-workers. In their careful study, it appears that measurable differences in the quantified gaseous species were not deduced. In the setup described herein, the availability of additional surface area between gaseous products and the sample is of concern, and determining the extent of catalytic effects is warranted.

DATA REDUCTION PROCEDURE

In order to deduce the species concentration from the acquired spectra, it is necessary to correct for the finite spectral resolution of the spectrometer [11, 12]. Procedures for correcting such spectra are available, and they will only be briefly outlined. In the developed model, account is made for both line and band structures of the molecular gases. Species considered in this work and their spectral regions of appearance are specified in Table 1. The radiative properties of these molecules are included in the HITRAN database [13] and included in the developed model. Several diatomic species, such as N_2, H_2, and O_2, are IR-inactive and not quantified. The computational procedure first involves a specification of the total pressure, measured temporal temper-

TABLE 1

Summary of Wavenumber Ranges Used in Data-Reduction Model

Range (cm^{-1})	Molecule	Comments
705–725	HCN (ν_2 band)	Vibrational bending bands of numerous molecules interfere with this strong HCN band.
900–1000	NH_3 (ν_2 band)	
1250–1375	HNO_3 (ν_3, ν_4, and $\nu_8 + \nu_9$ bands) N_2O (ν_1 band)	*P*-branches of HNO_3 slightly interfere with *R* branch of N_2O.
1565–1650	NO_2 (ν_3 band) H_2O (ν_2 band)	Weak NH_3 band interferes with spectra in this range. High H_2O concentrations will make NO_2 difficult to detect. Interference from atmospheric H_2O in background leads to uncertainty in H_2O and NO_2.
1680–1750	HNO_3 (ν_2 band) H_2O (ν_2 band, *R*-branch) CH_2O (ν_2 band) NH_3 (ν_4 band)	CH_2O not in current version of HITRAN data base. Need high NH_3 concentrations for detection.
1880–2140	NO (ν_0 band, *R*-branch) CO (ν_0 band, *P*-branch)	NO and CO have well-defined band structures.
2140–2250	CO (ν_0 band, *R*-branch) N_2O (ν_3 band)	*P*-branch of N_2O interferes with *R*-branch of CO.
2320–2380	CO_2 (ν_3 band, *R*-branch)	Strong absorption band of CO_2.
2740–3940	CH_2O (ν_1, ν_4, and $2\nu_3$ bands)	Weak absorption bands of CH_2O. C—H stretching bands from other molecules, like C_2H_4, occur in this range.
3500–3750	H_2O (ν_1 and ν_3 bands) CO_2 ($2\nu_2 + \nu_3$ and $\nu_1 + \nu_3$ bands)	Interference from atmospheric H_2O and CO_2 in background leads to uncertainty in CO_2 and H_2O.

ature profile of the evolved gases, assumed path length, partial pressures, and coefficients for linear baseline shifts. A linear baseline shift is sometimes needed since small droplets could be ejected when the thermolysis temperature is high. The data-reduction routine uses a nonlinear, least-squares fitting method [14] to iteratively fit the measured spectral transmittance to the theoretical spectral transmittance. When the iterations are successfully completed, the relative concentrations of various species such as CO, NO, H_2O, CO_2, NO_2, HCN, C_2H_2, CH_4, and N_2O are obtained for each spectrum.

The theory employed in the data-reduction model assumes that Beer's law is applicable. As a result, the convolution of the true transmittance with the instrument line shape gives the measured spectral transmittance $\tau_m(\nu_n)$ and is expressed as

$$\tau_m(\nu_n) = \frac{I_{\text{det}}}{I_{0,\text{det}}} = \frac{\int_0^\infty \tau_t(\nu) f(\nu - \nu_n)\, d\nu}{\int_0^\infty f(\nu - \nu_n)\, d\nu} \quad (1)$$

where f is the instrument line shape, τ_t is the true spectral transmittance associated with IR-active gases, and ν_n is the wavenumber at a measured data point. Triangular apodization is used in the inverse Fourier transform of the data in the frequency domain, resulting in an instrument line shape given by

$$f(\nu - \nu_n) = \frac{\Delta_{\max} \sin^2[\pi \Delta_{\max}(\nu - \nu_n)]}{[\pi \Delta_{\max}(\nu - \nu_n)]^2} \quad (2)$$

where $\Delta_{\max}$ is the maximum retardation of the moving mirror. Because of the oscillatory nature of the instrument line shape, the numerical evaluation of the integral in the numerator of Eq. 1 becomes computationally intensive. The true spectral transmittance can be expressed as

$$\tau_t(\nu) = \prod_i \prod_j \exp\big[- S_{i,j}(\nu_{0,i,j}, T) \times g(\nu - \nu_{0,i,j}, T) N P_i L \big], \quad i = 1, \ldots, N_s,\ j = 1, \ldots, N_r \quad (3)$$

where $S_{i,j}(\nu_0, T)$ is the line intensity for the ith species and jth rotational line, $g(\nu - \nu_{0,i,j}, T)$ is the line shape, $\nu_{0,i,j}$ is the frequency at the line center, N is the molecular number density, P_i is the partial pressure of the ith absorbing species, L is the optical path length, N_s is the number of absorbing species, and N_r is the number of rovibrational transitions. Since path length or volume occupied by the evolved gases is somewhat uncertain, results of the relative species concentrations are determined. At atmospheric pressures, collision broadening of the individual spectral lines is dominant. Hence, a Lorentzian line shape is employed. Data on the half-width-at-half-height of the spectral line are taken from the HITRAN database [13] and used without further modification. In addition, it should be noted that overlapping of spectral lines from the same and different molecules is considered in Eq. 3.

DISCUSSION OF RESULTS

To illustrate typical results obtained by using CRT/FTIR spectroscopy, the heating rates with and without a sample as well as the thermal decomposition characteristics of three different energetic materials are considered. These energetic materials are cyclotetramethylenetetranitramine (HMX), RDX, and hydroxylammonium nitrate (HAN). First, we illustrate the achievable heating rates.

Heating Rates

The heating rates that can be achieved by this system at different set temperatures (T_{set}) were measured, and the results are shown in Fig. 4. The measurement of heating rates was performed by using a 25 μm K-type thermocouple with and without an inert sample. An attempt was made to position the bead of the thermocouple in close vicinity of sample holder. Inspection of Fig. 4 reveals several different features. Each temperature trace exhibits two different slopes due to the unique heating mechanism during the measurement. The first, relatively small slope is due to the lower heater probe's contact with the sample holder and

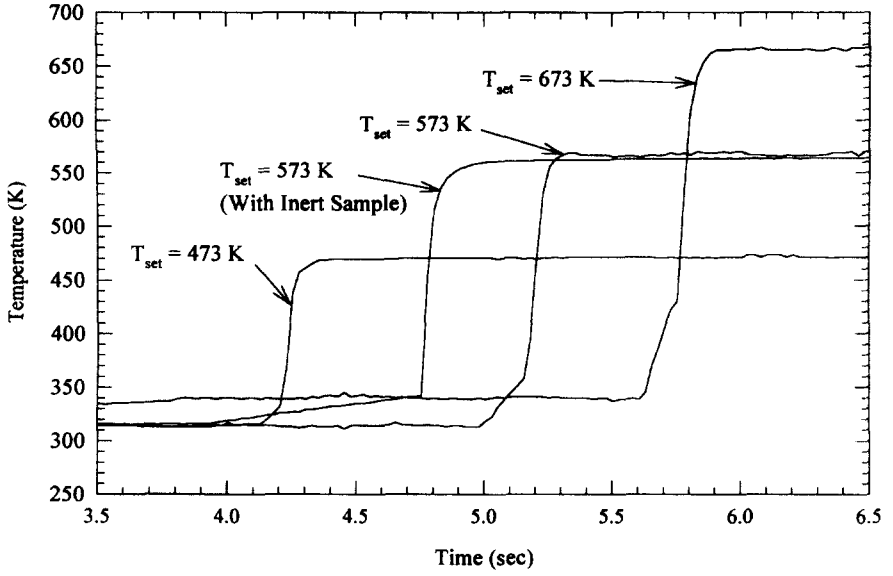

Fig. 4. Measurement of temperature response using a 25μm *K*-type thermocouple without a sample and with an inert sample (about 1 mg of a conductive silicone paste) at a single set temperature.

thermocouple during the pneumatically controlled upward motion. The second, steep slope represents the high heating rate that is achieved when the two heater probes have made a proper contact with each other. A heating rate of about 1500 K/s was achieved for this situation. However, a higher heating rate could be obtained as the set temperature increased. Third, the slightly higher initial temperature recorded for the 673 K temperature trace is caused by convective heat transfer from the lower heater. Measurement of the heating rate was also performed using about 1 mg of an inert material, conductive silicone paste (OMEGATHERM 201). The bead of the thermocouple was positioned within the paste on the sample holder with T_{set} = 573 K. Since the sample mass is relatively small compared to the mass of the two heaters, the sample mass did not cause a decrease in the heating rate. In fact, the recorded heating rate was increased by using the inert sample due to the enhanced contact between the fine-wire thermocouple and the two foils. It should be noted that only the foil attached to the sample holder is initially relatively close to the ambient temperature; the foil attached to the upper heater is initially at T_{set}.

Thermal Decomposition of HMX and RDX

The results from numerous thermal decomposition studies are available in the literature on the two cyclic nitramines RDX and HMX, but it appears that only a few subjected the sample to high heating rates. Boggs [15] and Adams and Shaw [16] have provided a summary on the thermal behavior from various studies of these materials. However, since then, many additional works have appeared, the results of which have been incorporated in modeling activities [1–3]. At standard temperature and pressure, both of these compounds exist in a crystalline state; liquefaction occurs at 478 and 558 K for RDX and HMX, respectively.

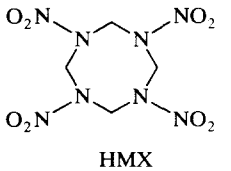

HMX

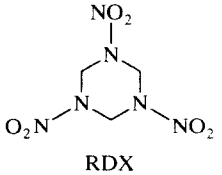

RDX

In recent research efforts on these nitramines, the emphasis has been put on providing an insight into the decomposition behavior and deducing the appropriate kinetic rates. However, it appears that condensed-phase decomposition is quite limited for steady-state defla-

gration of RDX [1, 2], but this may not be the case for HMX due to its higher melting temperature. It is clear, however, that reactions in the primary reaction zone in the immediate vicinity of the surface, primarily between H_2CO and NO_2, exert a strong influence on the burn rate for propellants containing these ingredients.

In view of the highly complex structure of these molecules, it is challenging to elucidate the chemical kinetic details during rapid thermolysis. As a result, it has been difficult to formulate a thermal decomposition model of these compounds for use in simulation of self-sustained, steady deflagration [1] or laser-assisted ignition and combustion [2]. The decomposition products are present in the primary reaction zone, and its thickness is on the order of 10–50 μm involving temperature gradients on the order of 10^3 K/mm [17]. Recent studies [4, 18–21] have shown that the overall decomposition pathways of HMX and RDX can be described by the following two competitive reactions:

$$\text{HMX(RDX)} \begin{cases} \rightarrow 4(3)[N_2O + CH_2O] & \text{(R1)} \\ \rightarrow 4(3)[\text{HONO} + \text{HCN}] \text{ or} & \\ \rightarrow 4(3)[NO_2 + \text{HCN} + \text{H}]. & \text{(R2)} \end{cases}$$

For HMX, reaction (R1) is exothermic by -209 kJ/mol, and reaction (R2) is endothermic by 159 kJ/mol. The global decomposition of bulk HMX is therefore almost thermally neutral, but it also depends on the kinetic rates at the considered temperature. The two competitive reaction pathways for HMX have been defined as subglobal reactions because many elementary reactions that occurred during the decomposition process were embedded in these two reactions. For example, early in the event, NO_2 and N_2O were detected before HCN and CH_2O evolved, whereas reactions (R1) and (R2) suggest a simultaneous evolution [4, 18]. Simultaneously with the evolution of HCN and CH_2O, a small amount of CO_2 was also detected among the gaseous decomposition products. However, a slight fluctuation in the species concentration profiles was obtained due to the bubble formation in the condensed phase and mixing of the decomposition products with the cool purge gas. During the final stage of the decomposition process, the relative concentrations of N_2O and CH_2O appeared in about the same amount as NO_2 and HCN, providing strong support for the validity of reactions (R1) and (R2). If these two reactions are thermally neutral and their rates are about the same, a large amount of heat evolved from decomposition and combustion of HMX must come from secondary reactions in the near-surface zone. The most important gas-phase reaction appears to be the following global reaction:

$$CH_2O + NO_2 \rightarrow CO + NO + H_2O \qquad \text{(R3)}$$

whose kinetic rate has been determined in shock-tube experiments [22].

In order to compare results obtained by other experimental methods with those obtained by CRT/FTIR spectroscopy, we show in Figs. 5 and 6 the evolution of the species concentrations at temperatures of 573 and 623 K, respectively. It should be noted that the species concentrations were not normalized by the sum of all species concentrations. The same path length in Eq. 3 was used in the data reduction. There are several interesting features in these figures. First, the induction time (time elapsed up to species evolution) decreased from about 1.45 s at 573 K to about 0.83 s at 623 K. These times are shorter compared to those recorded by Brill [18]. Second, Fig. 5 shows that the evolution of N_2O and CH_2O occurs at quite similar high rates, whereas the other species evolve at much lower rates. The faster evolution rate of these two species involves the low-temperature decomposition pathway mentioned previously, which appears to be dominant at 573 K. At the beginning of the thermal decomposition of HMX at 573 K, each species started to evolve at different times. A small amount of N_2O was detected first, and was followed by CO_2 and NO_2. About 1.2 s later from the first detection of N_2O, CH_2O started to appear, and was followed by HCN. A small amount of CO and NO was also detected in the later stage of the decomposition process. The formation of NO and CO was possibly caused by the gas-phase reaction (R3) and reactions of NO_2 with highly reactive radicals, such as HCO. NO formation can also be due

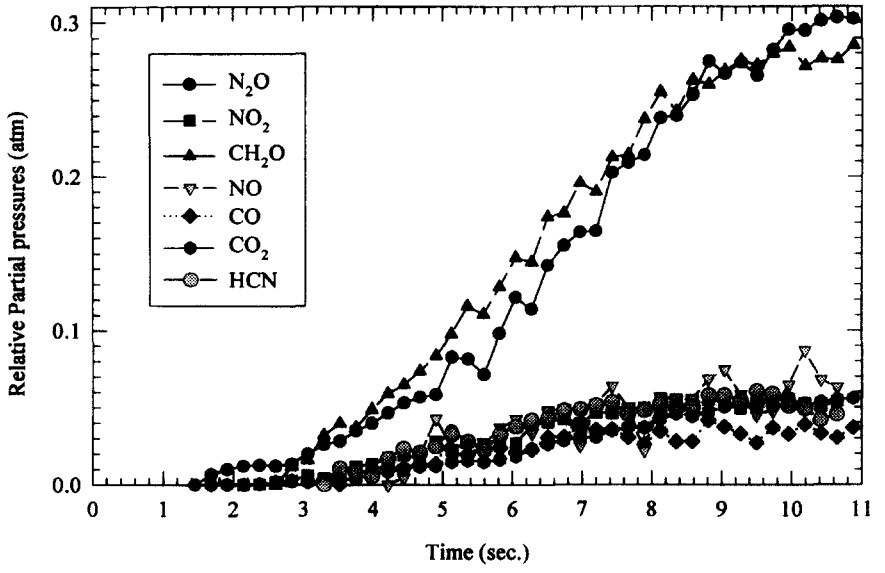

Fig. 5. Evolution of species concentrations during thermal decomposition of HMX at a set temperature of 573 K and a nitrogen environment at 1 atm.

to reaction pathways involving HONO, which is not quantified. Species formed at a much slower rate include HCN, NO_2, NO, CO, and CO_2. However, during the thermal decomposition of HMX at 623 K, N_2O, CH_2O, NO_2, and HCN are detected at about the same time and appear in similar concentrations, as shown in Fig. 6. This indicates that the high- and low-temperature decomposition pathways are about thermally neutral at this high temperature. At 575 K, the ratio of N_2O and NO_2 was lower because the low-temperature reaction was

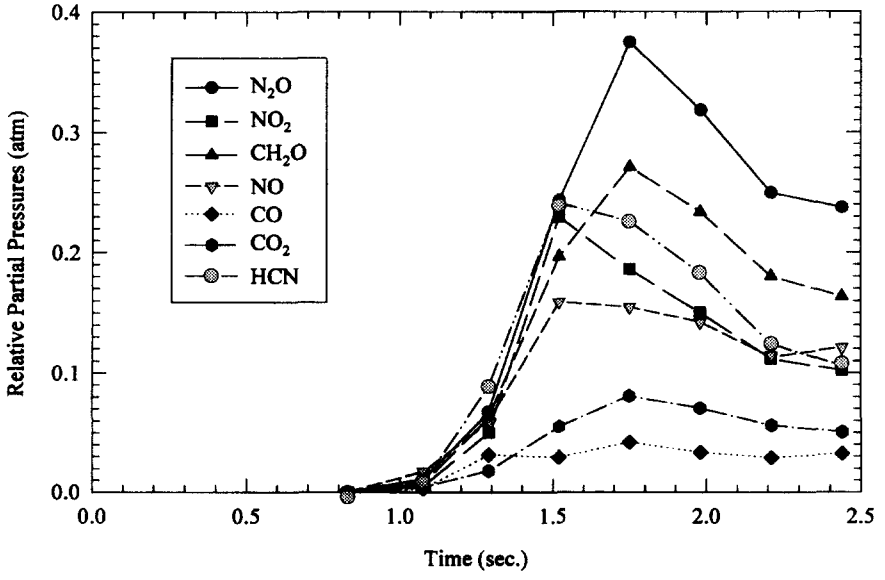

Fig. 6. Evolution of species concentrations during thermal decomposition of HMX at a set temperature of 623 K and a nitrogen environment at 1 atm.

more favorable. The results from T-jump/FTIR spectroscopy yielded a large amount of NO after the highly exothermic reaction between CH_2O and NO_2 [18]. Similarly, a relatively high concentration of NO was also detected in this experiment. A small quantity of CO_2 was also detected due to secondary reactions. The observed species evolution profiles are also similar to those observed by Behrens [23], and Behrens and Bulusu [24], who used time-of-flight mass spectroscopic techniques at lower temperatures and much lower heating rates. Consequently, the results obtained from this experiment agree reasonably well with the description of HMX decomposition using the proposed two competitive reaction pathways.

To develop either a detailed or global decomposition mechanism of complex energetic materials, such as HMX, the measurement should include as many species as possible. In the case of FTIR spectroscopy, one is limited to species which are IR-active, and to some extent to species whose spectral absorption coefficient has been quantified. To further guide the development of reaction mechanisms, it is useful to show the evolution of the element fractions. For HMX, whose chemical formula can be written as $(CH_2NNO_2)_4$, those ratios are plotted in Figs. 7 and 8, corresponding to the species evolution profiles described previously. Since this experiment is a transient one, it is not necessary that the element fractions should evolve as O, N, H = 0.286, and C = 0.142 and be independent of time. If no residue is formed on the foil, the element fractions integrated over time should, however, equal these theoretical ones if all species could be detected. Examination of these figures reveals that both the O-, N-, and C-atom balances are close to the theoretical ones, and should be considered as quite satisfactory. Species containing H atoms appear to be missing from the measurement. These include H_2 and H_2O, but spectral features due to water were indeed quite small. Additional species not quantified but appearing in the decomposition of HMX include HNCO and HONO; further work regarding the development of a database containing the spectral absorption coefficient for these two species is needed. In addition, a small amount of a nonvolatile residue remains on the foil [23, 24].

The species evolution profiles for RDX at thermolysis temperatures of 548 and 600 K are shown in Figs. 9 and 10, respectively. The

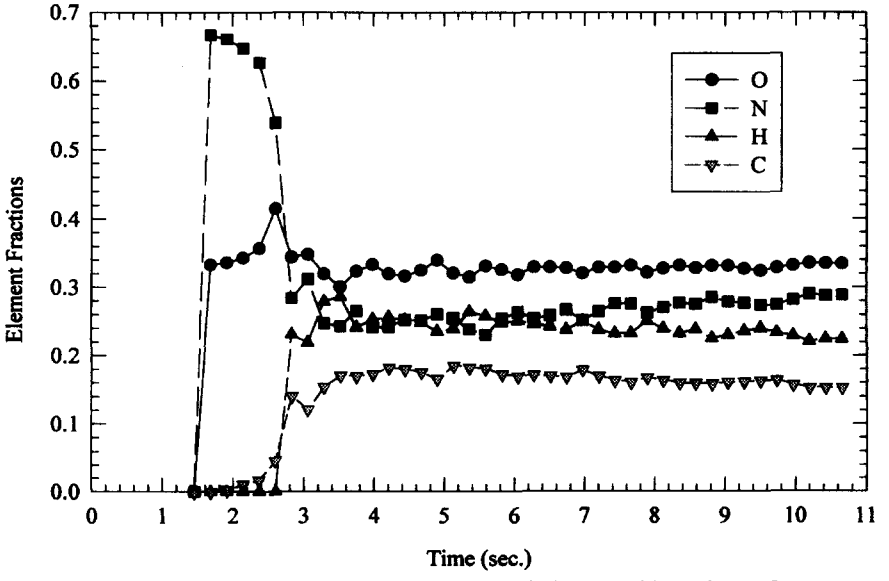

Fig. 7. Evolution of element fractions during thermal decomposition of HMX at a set temperature of 573 K and a nitrogen environment at 1 atm.

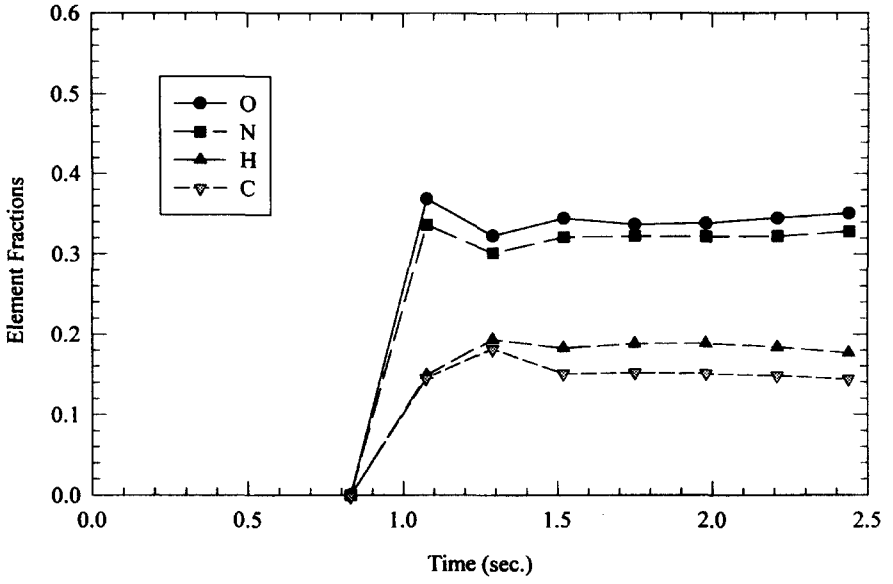

Fig. 8. Evolution of element fractions during thermal decomposition of HMX at a set temperature of 623 K and a nitrogen environment at 1 atm.

decomposition characteristics of RDX are similar to those of HMX [15, 16, 18]. The enthalpies of (R1) and (R2) for RDX are −121 and 159 kJ/mol, respectively. Therefore, the overall reaction could be considered as nearly thermally neutral, but its heat-release rate varies with temperature. The source of heat for further decomposition and reaction of RDX is the gas-phase reaction among CH_2O and NO_2 species. The species evolution profiles for RDX generated using CRT/FTIR spectroscopy showed similar trends compared to

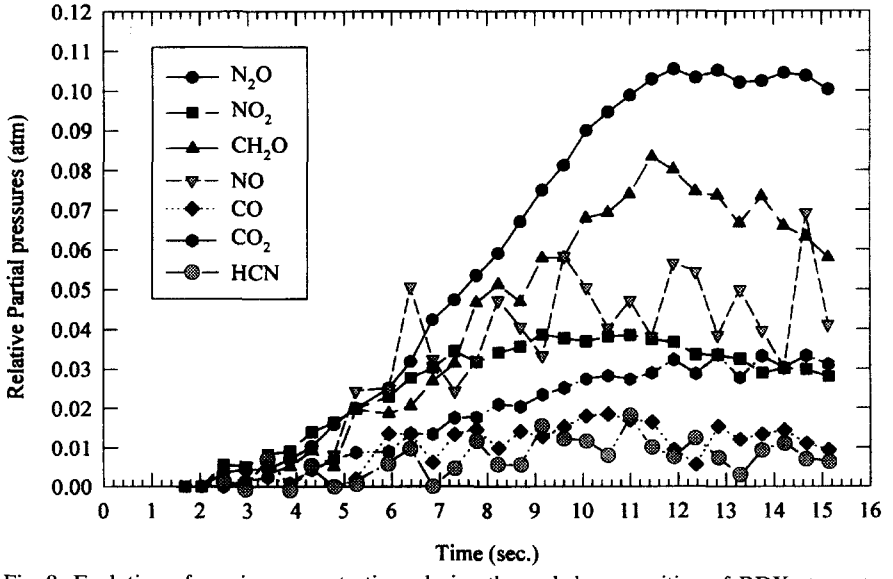

Fig. 9. Evolution of species concentrations during thermal decomposition of RDX at a set temperature of 548 K and a nitrogen environment at 1 atm.

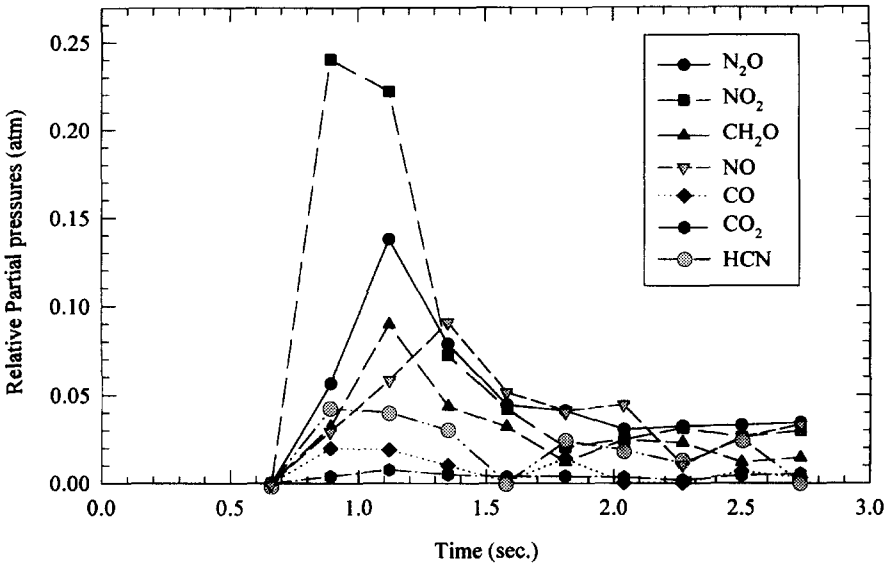

Fig. 10. Evolution of species concentrations during thermal decomposition of RDX at a set temperature of 600 K and a nitrogen environment at 1 atm.

those acquired for the decomposition of HMX. However, although T_{set} was lower compared to the experiments with HMX, a higher concentration of NO_2 was detected. A larger amount of NO_2 relative to N_2O evolved as T_{set} increased. For T_{set} = 600 K, the concentrations of N_2O and CH_2O were about same as the concentrations of HCN and NO_2. This indicated that the overall RDX decomposition process is almost thermally neutral at this temperature. However, at T_{set} = 548 K, only a small amount of HCN evolved due to the domination of low-temperature decomposition pathway.

Despite the similarity of the molecular structure between HMX and RDX, the species evolution profiles were, in general, different. It appears that the high-temperature decomposition pathway is more important for RDX compared to HMX for the considered temperatures. The corresponding element fraction profiles are shown in Figs. 11 and 12, corresponding to the species profiles shown in Figs. 9 and 10. It is evident in Figs. 11 and 12 that the element fraction balances are not as accurate compared to those shown in Figs. 7 and 8 for HMX. Missing species include H_2, N_2, H_2CN, HONO, and HNCO, as well as possibly larger fragments of RDX-like compounds.

Thermal Decomposition of HAN

HAN [$(NH_3OH)NO_3$] is a nitrate salt that exists as a solid at standard conditions [25–27]. It is considered as the oxidizer component in HAN-based liquid propellants. The burning behavior of HAN-based liquid propellants has been studied experimentally and theoretically. Vosen [28, 29] and McBratney and Vanderhoff [30] used liquid strand burners for visualizing the flame structure and deducing the burn rate. Zhu and Law [31] employed a heated liquid column method and high-temperature gases in the postcombustion region above a flat-flame burner in a study of individual droplets for characterizing the gasification and microexplosion processes. Kounalakis and Faeth [32] developed a one-dimensional analysis for predicting liquid surface properties and critical combustion pressures which are of interest for spray applications.

Since HAN contains both oxidizing and reducing elements, it is also a monopropellant. It decomposes at much lower temperatures compared to both HMX and RDX. At slow heating rates, the decomposition of HAN is known to be catalyzed by Fe and Cu [26]. At high heating rates, it appears that the gaseous product evolution is not affected in measurable quanti-

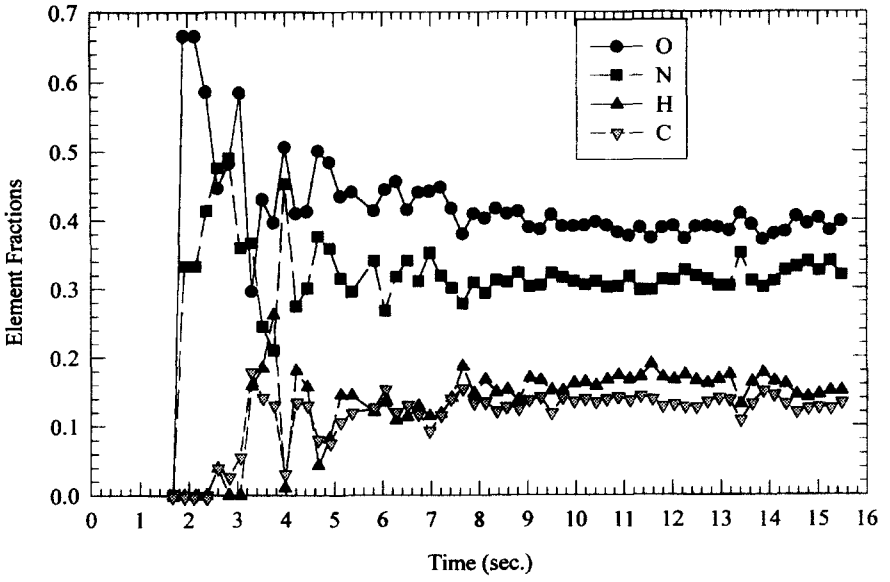

Fig. 11. Evolution of element fractions during thermal decomposition of RDX at a set temperature of 548 K and a nitrogen environment at 1 atm.

ties by the type of metal with which it makes contact. Based on our work, the differences in species evolution concentrations between the use of aluminum and SS304 foils are not quantifiable, possibly due to the short duration of the experiment. Such a finding is similar to the results of Cronin and Brill [26]. The species profiles from thermal decomposition of 13 M HAN (81% of HAN and 19% of water by weight) at 403 and 433 K using aluminum foils are shown in Figs. 13 and 14, respectively. In these cases, a syringe was employed to place an

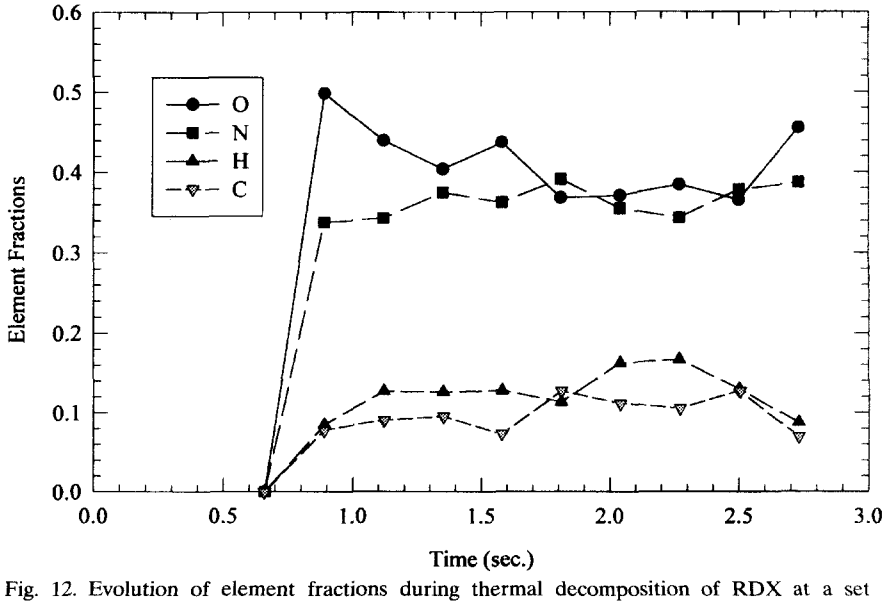

Fig. 12. Evolution of element fractions during thermal decomposition of RDX at a set temperature of 600 K and a nitrogen environment at 1 atm.

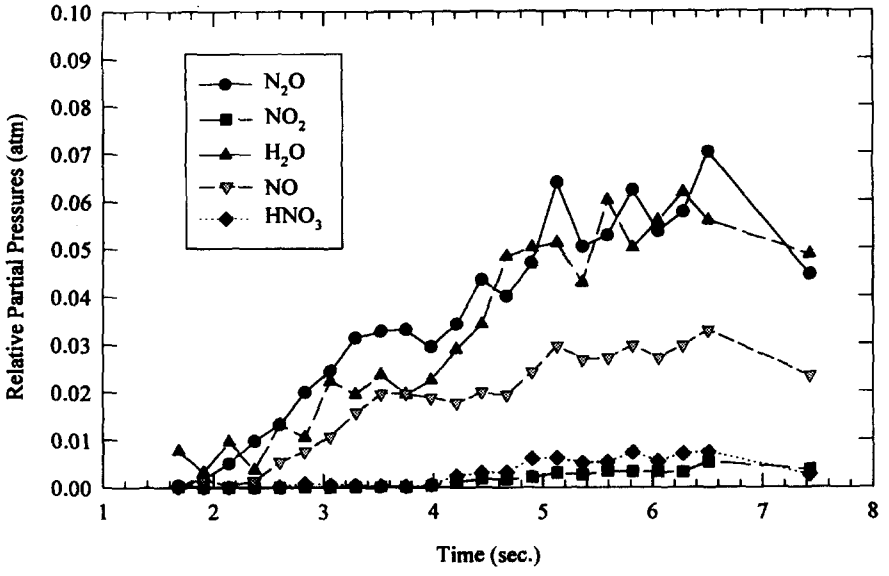

Fig. 13. Evolution of species concentrations during thermal decomposition of HAN at a set temperature of 403 K and a nitrogen environment at 1 atm.

8 μL droplet on the foil which was attached to the sample holder. The sample holder was placed on the lower guiding tube, and the chamber was closed. Normally, about 2 min or less elapsed between placing the sample holder on the guiding tube and the start of thermolysis of sample. There are several interesting features present in Figs. 13 and 14.

First, the induction time is about 1.8 and 1.2 s for thermolysis temperatures of 403 and 433 K, respectively. Here, we define the induction time as the time to evolution of reactive species. With the spectrometer set to collect spectra at 2 cm^{-1} spectral resolution, the induction time is measured with an uncertainty of approximately 0.23 s. The difference in the

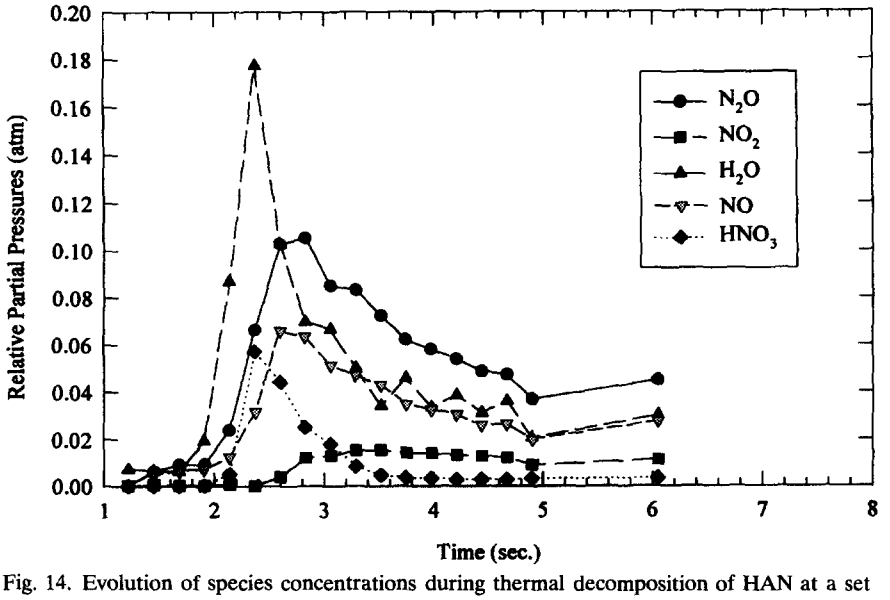

Fig. 14. Evolution of species concentrations during thermal decomposition of HAN at a set temperature of 433 K and a nitrogen environment at 1 atm.

induction time is about three times the uncertainty of the measurement. It is evident that N_2O evolves in largest concentration among the reactive species, and its detection signals the end of the induction time. At 433 K, H_2O is initially detected as the major species due to strong evaporation. In addition, no detectable gases are present within the modulated beam of the FTIR spectrometer prior to the induction time.

The chemical kinetic events that occur prior to the evolution of gaseous species are complex, and involve multiple steps and pathways [27]. First, proton transfer in HAN is probably the dominant mechanism for the formation of HNO_3. The acid subsequently decomposes in the condensed phase to form the important nitronium ion (NO_2^+) and hydroxide ion (OH^-) which are active within the condensed phase:

$$HAN \rightarrow NH_2OH + HNO_3 \qquad (R4)$$

$$HNO_3 \rightarrow NO_2^+ + OH^- . \qquad (R5)$$

The highly reactive species are not quantified. It is thought that the nitronium ion and the hydroxide ion are subsequently involved in the following reactions:

$$NH_2OH + NO_2^+ \rightarrow H_2NO^+ + HONO \qquad (R6)$$

$$H_2NO^+ + OH^- \rightarrow H_2O + HNO . \qquad (R7)$$

Once HONO and HNO build up in large concentrations, the induction period is near its completion, and NO and N_2O as well as water evolve into the gas-phase region and are detected. The formation of these species could come from an HONO and HNO attack on HAN via the global steps

$$HONO + HAN \rightarrow N_2O + 2H_2O + HNO_3 \qquad (R8)$$

$$HNO + HAN \rightarrow N_2 + 2H_2O + HNO_3 . \qquad (R9)$$

Figure 14 shows that HNO_3 first rapidly evolves, and then rapidly disappears. The rapid disappearance could indicate that most of the dissolved HAN has been consumed. As a result, it is suggested that further depletion of HONO is through an attack on HNO_3 according to the global reaction

$$HONO + HNO_3 \rightarrow H_2O + 2NO_2 \qquad (R10)$$

since the detection of NO_2 follows that of the disappearance of HNO_3. At low temperatures, N_2O also appears in large concentrations, but its evolution lags that of water. At 433 K, NO evolves in concentrations that are similar to the concentration of H_2O. This is clearly by far the most surprising result. The evolution of NO seems to suggest that nitrous acid (HONO) and the nitroxyl (HNO) are rapidly eliminated by reactions involving HONO [27 and references therein]:

$$2HONO \rightarrow NO + NO_2 + H_2O \qquad (R11)$$

$$HONO + HNO \rightarrow 2NO + H_2O . \qquad (R12)$$

In general, HONO and HNO appear in a wide variety of reaction steps and pathways, and a consideration of these species is needed in the development of a reaction mechanism of HAN. In addition, no residue remains on the surface of the foils, and visually there appears to be no staining or pitting of the surface.

Based on the preceding discussion of HAN decomposition, it is evident that HONO and HNO play an important role. However, these species in addition to N_2 are not quantified in Figs. 13 and 14. Since the 13 M HAN solution can be written as $N_{0.15}O_{0.38}H_{0.47}$, the element fraction profiles shown in Figs. 15 and 16 suggest that several important species are indeed missing in the data reduction. The atom balance for N is overestimated by a factor of 2, whereas H is underestimated by a factor of almost 2, whereas the O-element balance appears reasonable. It should be noted that the transient effect should also be considered. The deficiencies in element fraction profiles could be caused by underestimated mole fractions of H_2O, which condensed out as it evolved into the probe volume of the FTIR where the measured temperature was below 343 K.

SUMMARY

An experimental facility for performing high heating rate thermolysis studies of energetic materials is described. The evolved gaseous

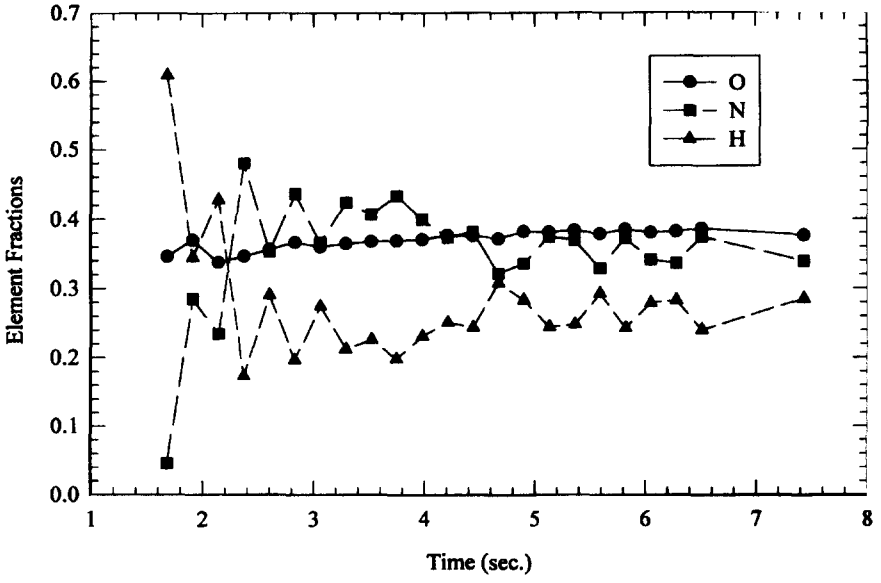

Fig. 15. Evolution of element fractions during thermal decomposition of HAN at a set temperature of 403 K and a nitrogen environment at 1 atm.

products are quantified using FTIR absorption spectroscopy. The acquired absorption spectra are utilized for obtaining the species concentration by correcting for the finite spectral resolution of the spectrometer. Representative results from confined isothermal decomposition studies of HMX, RDX, and HAN are described in detail. It is demonstrated that heating rates exceeding 1500 K/s can be achieved by utilizing a small amount of the sample. Regarding HMX and RDX, the evolved species products are quite similar to

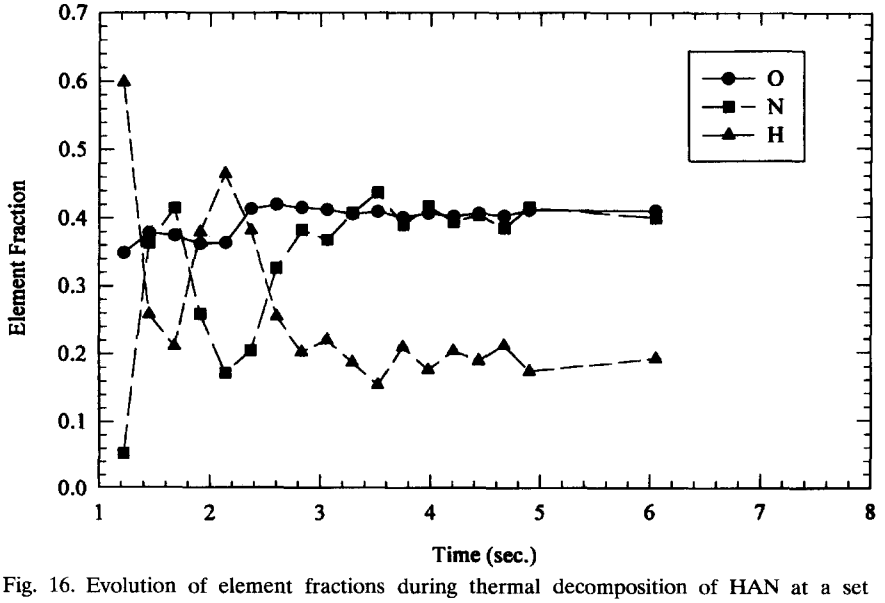

Fig. 16. Evolution of element fractions during thermal decomposition of HAN at a set temperature of 433 K and a nitrogen environment at 1 atm.

those that have been previously described in the literature. It appears, however, that the rates of the two global decomposition pathways are somewhat different for these two cyclic nitramines. CRT/FTIR spectroscopy of a liquid monopropellant (13M HAN) has also been performed. The results show that N_2O is the dominant reactive species formed, and that water appears in large concentrations early in the event due to evaporation. It is conjectured that HONO and HNO are important intermediates in HAN decomposition, and attempts should be made to quantify these species, as well as several important IR-active species relevant to decomposition of nitramines.

The studies on RDX and HMX were performed under Contracts DAAL03-92-G-0020, DAAL03-92-G-0118, and DAAH04-94-G-0202 with support from Drs. D. M. Mann and R. W. Shaw of the U.S. Army Research Office, Research Triangle Park, NC. The study on HAN was performed under Contracts DAAE30-95-C-0009 and DAAE30-96-C-0057 with support from Mr. R. Wisser and Mr. J. Irizarry, respectively, of the U.S. Army Research, Development, and Engineering Center, Picatinny Arsenal, NJ. We are grateful to Mr. Sandy Moore of Olin for supplying the samples of HAN used in this study.

REFERENCES

1. Liau, Y.-C., and Yang, V., *J. Prop. Power* 11:729–739 (1995).
2. Prasad, K., Smooke, M., and Yetter, R. A., *Proceedings of the 32nd JANNAF Combustion Subcommittee Meeting*, CPIA, 1995.
3. Yetter, R. A., Dryer, F. L., Allen, T., and Gatto, J., *J. Prop. Power* 11:666–676 (1995).
4. Brill, T. B., *J. Prop. Power* 11:740–751 (1995).
5. Brill, T. B., Arisawa, H., Brush, P. J., Gongwer, P. E., and Williams, G. K., *J. Phys. Chem.* 99:1384–1392 (1995).
6. Oyumi, Y., and Brill, T. B., *Combust. Flame* 62:213–224 (1985).
7. Timken, M. D., Chen, J. K., and Brill, T. B., *Appl. Spectrosc.* 44:701–706 (1990).
8. Brill, T. B., Brush, P. J., James, K. J., Shepherd, J. E., and Pfeiffer, K. J., *Appl. Spectrosc.* 46:900–911 (1992).
9. Thynell, S. T., Gongwer, P., and Brill, T. B., *J. Prop. Power* 12:933–939 (1996).
10. Mallery, C. F., Kim, E. S., and Thynell, S. T., *Rev. Sci. Instrum.* 66:4091–4094 (1995).
11. Anderson, R. J., and Griffiths, P. R., *Anal. Chem.* 47:2339–2347 (1975).
12. Griffiths, P. R., and de Haseth, J. A., *Fourier Transform Infrared Spectrometry*, Wiley, New York, 1986.
13. Rothman, L. S., et al., *J. Quant. Spectrosc. Radiat. Transfer* 48:469–507 (1992).
14. Press, W. H., Teukolsky, S. A., Vetterling, W. T., and Flannery, B. P., *Numerical Recipes*, Cambridge University Press, Cambridge, 1992, pp. 650–700.
15. Boggs, T. L., in *Fundamentals of Solid Propellant Combustion* (K. Kuo and M. Summerfield, Eds.), Vol. 90, Progress in Astronautics and Aeronautics Series, AIAA, New York, 1984, pp. 121–175.
16. Adams, G. F., and Shaw, R. W., Jr., *Annu. Rev. Phys. Chem.* 43:311–340 (1992).
17. Parr, T., and Hanson-Parr, D., in *Nonsteady Burning and Combustion Stability of Solid Propellants* (L. De Luca, E. W. Price, and M. Summerfield, Eds.), Vol. 143, Progress in Astronautics and Aeronautics Series, AIAA, New York, 1992, pp. 261–324.
18. Brill, T. B., and Brush, P. J., *Philos. Trans. R. Soc. London, Ser. A* 339:377–385 (1992).
19. Huang, T. H., Thynell, S. T., and Kuo, K. K., *J. Prop. Power* 11:781–790 (1995).
20. Melius, C. F., in *Chemistry and Physics of Energetic Materials* (S. Bulusu, Ed.), Kluwer Academic, Norwell, MA, 1990, pp. 21–78.
21. Brill, T. B., in *Chemistry and Physics of Energetic Materials* (S. Bulusu, Ed.), Kluwer Academic, Norwell, MA, 1990, pp. 255–276.
22. Lin, C.-Y., Wang, H.-T., Lin, M. C., and Melius, C. F., *Int. J. Chem. Kinet.* 22:455–482 (1990).
23. Behrens, R., *J. Phys. Chem.* 94:6706–6718 (1990).
24. Behrens, R., and Bulusu, S., *J. Phys. Chem.* 95:5838–5847 (1991).
25. Cronin, J. T., and Brill, T. B., *J. Phys. Chem.* 90:178–191 (1986).
26. Cronin, J. T., and Brill, T. B., *Combust. Flame* 74:81–89 (1988).
27. Klein, N., *Proceedings of the 27th JANNAF Combustion Meeting*, CPIA Publ. 557, 1990, Vol. I, pp. 443–450.
28. Vosen, S. R., *Twenty-Second Symposium (International) on Combustion*, The Combustion Institute, Pittsburgh, 1988, pp. 1817–1825.
29. Vosen, S. R., *Combust. Flame* 82:376–388 (1990).
30. McBratney, W. F., and Vanderhoff, J. A., ARL-TR-442, Army Research Laboratory, Aberdeen Proving Ground, MD, 1994.
31. Zhu, D. L., and Law, C. K., *Combust. Flame* 70:333–342 (1987).
32. Kounalakis, M. E., and Faeth, G. M., *Combust. Flame* 74:179–192 (1988).

Received 29 March 1996